Monthly Notices of the ROYAL ASTRONOMICAL SOCIETY

MNRAS **552,** 1–7 (2026)
https://doi.org/10.1093/mnras/stag1907
Advance Access publication 2026 October 7
Letter

Shortening the baseline: characterising Type Ia supernovae using $\Delta m_{10}(X)$

Joel M. Velasco [1]★ Paolo A. Mazzali [1,2] Christopher Ashall [3] Christopher R. Burns [4] Mark M. Phillips [5] Lluis Galbany [6,7] Nidia Morrell [5] Maximilian D. Stritzinger [8] Peter Hoeflich [9] Eric Y. Hsiao [9] and Syed A. Uddin [10,11]

[1]*Astrophysics Research Institute, Liverpool John Moores University, IC2, Liverpool Science Park, 146 Brownlow Hill, Liverpool L3 5RF, UK*
[2]*Max-Planck-Institut für Astrophysik, Karl-Schwarzschild-Str 1, D-85748 Garching, Germany*
[3]*Institute for Astronomy, University of Hawaii, 2680 Woodlawn Dr, Honolulu, HI 96822, USA*
[4]*Observatories of the Carnegie Institution for Science, 813 Santa Barbara St, Pasadena, CA 91101, USA*
[5]*Carnegie Observatories, Las Campanas Observatory, Colina El Pino, Casilla 601, Chile*
[6]*Institute of Space Sciences (ICE-CSIC), Campus UAB, Carrer de Can Magrans, s/n, E-08193 Barcelona, Spain*
[7]*Institut d'Estudis Espacials de Catalunya (IEEC), E-08860 Castelldefels (Barcelona), Spain*
[8]*Department of Physics and Astronomy, Aarhus University, Ny Munkegade 120, DK-8000 Aarhus C, Denmark*
[9]*Department of Physics, Florida State University, 77 Chieftan Way, Tallahassee, FL 32306, USA*
[10]*Center for Astronomy, Space Science and Astrophysics, Independent University, Bashundhara R/A, Dhaka 1229, Bangladesh*
[11]*American Public University System, 111 W. Congress St, Charles Town, WV 25414, USA*

Accepted 2026 October 5. in original form 2026 September 7

ABSTRACT

An explorative study of Type Ia supernovae (SNe Ia) light curves is presented. $\Delta m_t(X)$ decline-rate metrics are used to evaluate alternative characterisations of light-curve diversity and the luminosity–width relation (LWR). Using a sample of 362 SNe Ia from the Carnegie Supernova Project (CSP-I and CSP-II), Gaussian process regression is used to fit *B*- and *g*-band light curves and measure decline-rates across multiple post-maximum time-scales. The LWR is calibrated using a clean subsample of SNe Ia with host-independent distance moduli and Fitzpatrick (1999) reddening corrections. Decline-rates $\Delta m_{10}(B)$ and $\Delta m_{10}(g)$ are found to capture the LWR effectively, while mitigating the severe degeneracy that affects longer time-scales for fast-declining ($\Delta m_{15}(B) \geq 1.6$ mag) events. Continuous, piecewise linear models are presented that seamlessly anchor the transition between normal and fast-declining regimes. The decline-rate $\Delta m_{10}(X)$ closely approximates the results of the more complex colour-stretch parameters, requiring less post-maximum temporal coverage than $\Delta m_{15}(B)$ or s_{BV}, and offers an even greater sensitivity for slow decliners. $\Delta m_{10}(B)$ provides a precise and practical tool for large-scale photometric surveys and real-time observer classification.

Key words: methods: data analysis – techniques: photometric – supernovae: general – cosmological parameters.

1 INTRODUCTION

Type Ia supernovae (SNe Ia) are luminous stellar explosions, which can be observed out to redshifts corresponding to a time when the Universe was half its present age (S. Perlmutter et al. 1998). SNe Ia have been utilised as indicators of extragalactic distance, thanks to the discovery that the rate of evolution of their light curves correlates with their intrinsic luminosity (I. P. Pskovskii 1977; M. M. Phillips 1993). They were instrumental in the discovery of the accelerated expansion of the Universe (A. G. Riess et al. 1998; S. Perlmutter et al. 1999). Despite this, much is yet to be learned about their physical properties, and even the nature of their progenitors (beyond the presence of at least one exploding carbon–oxygen white dwarf) is a matter of debate (F. Hoyle & W. A. Fowler 1960; B. Wang & Z. Han 2012; M. Livio & P. Mazzali 2018).

To correct for an apparent luminosity–width relation (LWR), M. M. Phillips (1993) devised a measure of the decline-rate, $\Delta m_{15}(B)$. Defined as the *B*-band magnitude difference from peak to 15 d later, this parameter has been crucial for characterising the intrinsic luminosity of SNe Ia and enabling their use as standard candles. Historically, the 15-d baseline was a practical compromise dictated by the photometric cadence of the Calan/Tololo survey, where shorter time-scales were not feasible (M. Hamuy et al. 1996). When applied alongside a colour–luminosity relation (R. Tripp 1998; A. G. Riess et al. 1999), SNe Ia can be standardised, reducing peak luminosity scatter to ∼0.15 mag (M. M. Phillips et al. 1999; S. Jha, A. G. Riess & R. P. Kirshner 2007). However, while this timebase captures the variance of most SNe Ia, it struggles to distinguish between the fastest-declining events.

★ E-mail: arijvela@ljmu.ac.uk

© The Author(s) 2026.
Published by Oxford University Press on behalf of Royal Astronomical Society. This is an Open Access article distributed under the terms of the Creative Commons Attribution License (https://creativecommons.org/licenses/by/4.0/), which permits unrestricted reuse, distribution, and reproduction in any medium, provided the original work is properly cited.

Downloaded from academic.oup.com/mnras/article/552/4/stag1907/8876083 by Sarah Dakin user on 05 November 2026

$\Delta m_{15}(B)$ exhibits a prominent breakdown at the faint, rapidly declining end of the luminosity distribution ($\Delta m_{15}(B) \geq 1.6$ mag; S. Taubenberger et al. 2008; G. Folatelli et al. 2010). These fast-declining, 1986G and 1991bg-like SNe Ia synthesise lower ^{56}Ni masses (P. A. Mazzali et al. 2007), leading to cooler ejecta, earlier Fe-group recombination, and severe line-blanketing by Ti II that rapidly depresses post-maximum B-band flux (P. A. Mazzali et al. 1997; A. Alburai et al. 2026). At $\Delta m_{15}(B) \geq 1.6$ mag, $\Delta m_{15}(B)$ becomes highly degenerate, with SNe Ia of comparable decline-rates spanning more than two magnitudes in absolute luminosity (C. R. Burns et al. 2014; M. M. Phillips & C. R. Burns 2017). The increasing difficulty of tracking luminosity over longer time-scales suggests there is some impact felt, even in the B band, from the onset of the secondary maximum (Velasco et al., in preparation). While the secondary maximum is conventionally associated with near-infrared wavelengths, our analysis reveals a suppressed decline extending into the optical bands. For the dimmest, fastest-declining SNe Ia, the colour turnover driven by early Fe-group recombination occurs as early as ∼13 d post-maximum. Because this transition takes place before the traditional 15-d measurement window for fast-decliners, $\Delta m_{15}(X)$ becomes fundamentally degenerate.

To address these degeneracies, other luminosity proxies have been developed, for instance the colour-stretch parameter, s_{BV} (C. R. Burns et al. 2014, 2018). This parameter successfully characterises SNe Ia across the full luminosity range by utilising the $(B-V)$ colour curve. To measure s_{BV} directly from light curves requires high-cadence, multiband photometry extending 50 d past the B-band maximum.

Given this state of affairs, it was natural to ask the question whether using a shorter time-scale to measure the decline-rate would eliminate contamination from the secondary maximum and remove the degeneracy at the rapidly declining end, while retaining sensitivity to the absolute magnitude for normal SNe Ia.

G. Folatelli et al. (2010) experimented with modifying $\Delta m_{15}(B)$, altering both time-scale and photometric band. However, the data set used was limited, containing only two fast declining SNe Ia. Similarly, P. Hoeflich et al. (2017) studied decline-rates measured at a variable times after maximum, stretching light curves prior to measuring their decline. Here, we experiment with the decline-rate $\Delta m_{15}(B)$, modifying the 15 d period, while also measuring declines in the g band. Employing modern data that include a greater number of SNe Ia from across the luminosity range, we aim to find alternative time-scales, which more accurately encapsulate the variety in SNe Ia light curves, without needing the larger temporal baseline of s_{BV} or fitting with light-curve templates.

2 DATA

The data used in this letter are from the Carnegie Supernova Project (CSP), with this sample spanning both CSP-I (K. Krisciunas et al. 2017) and CSP-II surveys (M. M. Phillips et al. 2018). The CSP-I data include the photometry of 133 SNe Ia observed between 2004 and 2009. A further 229 SNe Ia are from CSP-II observations, which took place from 2011 to 2015 (M. M. Phillips et al. 2018). For CSP-I and II, optical imaging was obtained with the Las Campanas Observatory Swope telescope, with each SN observed every 2–3 d up to 2–3 weeks past maximum light. Combining the data from CSP-I and CSP-II into one larger data set, a total of 362 SNe Ia are used for analysis here. Supplementary parameters

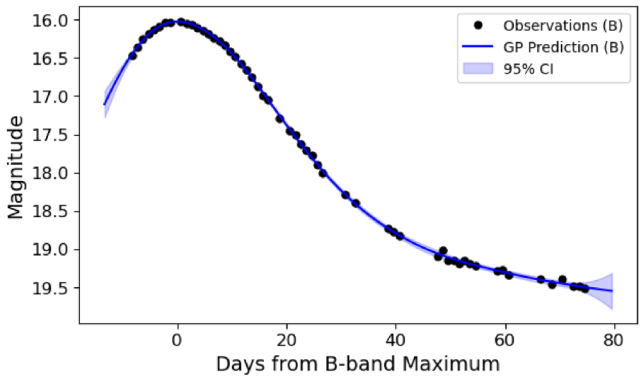


Figure 1. An example of a fitted light curve for SN2005M's B-band data. The black dots show the photometric data points and the blue line shows the GP fitted light curve, alongside a 95 per cent confidence interval around the fit.

for the host galaxies, specifically the colour excess $(E(B-V)_{\rm host})$ and the total-to-selective extinction coefficient $(R_{V,{\rm host}})$, were derived from multiwavelength template fits using SNOOPY (C. R. Burns et al. 2011, 2014; S. A. Uddin et al. 2024). Spectroscopic subclassifications were adopted from the literature. SNe Ia-91T were defined in M. M. Phillips et al. (2022), and 03fg-like SNe Ia (SNe Ia-03fg) were defined from C. Ashall et al. (2021).

In order to calibrate the absolute magnitudes of SNe Ia in the set, a calibration subsample of 23 CSP Ia events with reliable, redshift independent distance moduli was assembled. Cepheid distances were given priority, followed by tip of the red giant branch (TRGB), surface brightness fluctuations (SBF), and Tully–Fisher (TF) distances. Distance moduli were found using the Extragalactic Distance Database (R. B. Tully et al. 2009), with data taken from the SH0ES (A. G. Riess et al. 2022), Cosmicflows-4 (R. B. Tully et al. 2023), and HST IR SBF catalogues (J. P. Blakeslee et al. 2021; J. B. Jensen et al. 2021). For the remainder of the data set (the 'flow' sample), independent absolute magnitudes were computed from their cosmic microwave background (CMB) centric redshifts and the Hubble Law, assuming $H_0 = 73.04\,{\rm km\,s^{-1}\,Mpc^{-1}}$ (A. G. Riess et al. 2022).

3 METHODOLOGY

To ensure reliable decline-rate measurements, we required all SNe to possess photometric data prior to their respective band maximum. Because the peak must be well sampled to measure accurate decline-rates, we defined the epoch of maximum light using the peak of the fitted light curve rather than a single discrete data point, maximising the number of SNe eligible for analysis.

To preserve the true morphological heterogeneity of the SNe Ia, we refrained from using templates to measure the decline-rates. By directly fitting the photometric data points alone, the intrinsic nature of the SN light curve shape is preserved. A Gaussian process (GP) regressor, utilising a Matérn kernel, implemented via the SCIKIT-LEARN and SCIPY Python modules, was used to predict the shape of the light curves through probabilistic interpolation. All light curves were corrected for cosmological time dilation; K-corrections were deemed unnecessary given the low redshift of our sample ($z_{\rm max} < 0.14$), with around 75 per cent having $z < 0.05$. An example of a high-quality B-band light curve accurately fit by the GP model, alongside its 95 per cent confidence interval, is shown in Fig. 1.

Downloaded from academic.oup.com/mnras/article/552/4/stag1907/8876083 by Sarah Dakin user on 05 November 2026

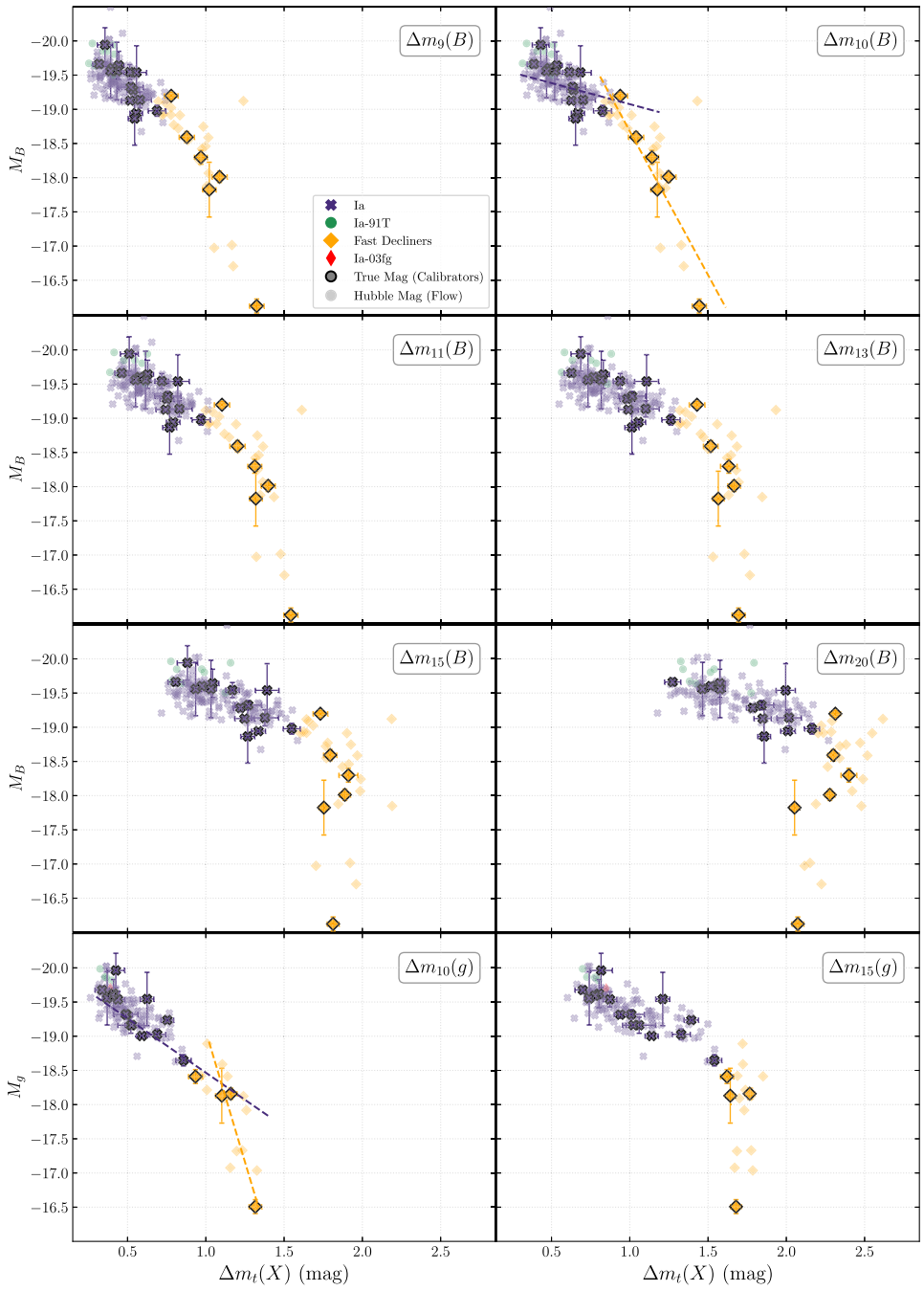


Figure 2. Absolute magnitude versus $\Delta m_t(X)$ for a variety of time-scales in both the B and g bands. True empirical calibrator SNe are highlighted with bold black outlines, while the larger 'flow' sample is plotted as a faded background distribution, using Hubble-derived distances. Error bars for the flow sample are omitted for visual clarity. The derived continuous piecewise linear models (dashed lines) are overlaid on the $\Delta m_{10}(X)$ panels.

From the GP fits, the time of maximum brightness in the B and g bands was extracted, allowing various decline-rates to be calculated. We determine uncertainties on $\Delta m_t(X)$ using a Monte Carlo approach based on the GP posterior. For each SN, we draw 100 random realisations from the GP fit, independently find the peak time ($t_{X,\max}$) for each iteration, and compute the resulting decline-rates. Taking the standard deviation across all 100 realisations maps the $t_{\max}$ covariance into the uncertainty.

Following the naming convention of G. Folatelli et al. (2010), these are referred to as $\Delta m_t(X)$, where t denotes the number of days since maximum X-band luminosity. $\Delta m_t(X)$ was computed for values of t from 8 to 20 d. Following the application of our selection criteria, we obtained B-band measurements for 224 SNe at $t = 8$ and 191 SNe at $t = 20$. In the g band, the yield ranged from 162 SNe at $t = 8$ to 153 SNe at $t = 20$.

Additionally, $(B{-}V)$ and $(g{-}r)$ colour curves were calculated to derive contemporary colour-stretch parameters. The $(B{-}V)$ curve was filtered for post-maximum epochs, and the time of the reddest point was extracted and divided by 30 to obtain s_{BV} (C. R. Burns et al. 2014, 2018). We measured s_{BV} directly for 81 SNe. For

Downloaded from academic.oup.com/mnras/article/552/4/stag1907/8876083 by Sarah Dakin user on 05 November 2026

the g band, the equivalent parameter s_{gr} (C. Ashall et al. 2021; the time of $(g-r)$ maximum relative to g-band maximum, normalised by 30 d) was computed for 76 SNe.

To calibrate the absolute magnitudes, we utilised the independent subsample of 23 calibrator SNe introduced in Section 2. Peak absolute magnitudes for these SNe were derived directly from the GP fits:

$$M_X = m_{X,\max} - \mu - A_{X,\mathrm{MW}} - A_{X,\mathrm{host}},$$

where $m_{X,\max}$ is the unreddened peak apparent magnitude. Total Galactic and host extinctions (A_X) were computed using the E. L. Fitzpatrick (1999) extinction law, assuming $R_V = 3.1$ for the Milky Way, alongside the host galaxy parameters ($E(B-V)_{\mathrm{host}}$ and $R_{V,\mathrm{host}}$) noted in Section 2. Milky Way colour excesses, $E(B-V)_{\mathrm{MW}}$, were obtained from E. F. Schlafly & D. P. Finkbeiner (2011) dust maps.

Using this calibrator sample, we constructed empirical LWRs for both the B and g bands. To accurately model the distinct photometric behaviour of fast-decliners without introducing discontinuities, we adopted an anchored, continuous piecewise linear fit. The transition into the fast-declining regime was empirically defined by the threshold $\Delta m_{15}(B) \geq 1.6$ mag (S. Taubenberger et al. 2008; G. Folatelli et al. 2010; C. Ashall et al. 2016). The slopes and transition points of these piecewise models were determined exclusively using the 23 calibrator SNe.

4 RESULTS

From these data, $\Delta m_{\,t}(X)$ decline-rates were plotted in order to infer their correlation with luminosity. This was in order to test for a reproduction of the LWR (M. M. Phillips 1993), while also analysing how the distribution changes for different values of t. Plots depicting absolute magnitude against $\Delta m_{\,t}(X)$ can be seen in Fig. 2.

The $\Delta m_{\,15}(B)$ plot appears as expected; for normal SNe Ia ($\Delta m_{15}(B) < 1.6$ mag), the decline-rate correlates reliably with peak luminosity. However, as the decline-rate crosses the $\Delta m_{15}(B) \approx 1.6$ mag threshold, this relationship breaks down entirely. The degeneracy caused by the fast-decliners means that assuming a luminosity from $\Delta m_{\,15}(B)$ alone for SNe with $\Delta m_{\,15}(B) > 1.6$ mag could lead to discrepancies greater than 2 mag. Such an uncertainty highlights the motivation and opportunity for another metric, one which maintains resolving power over a greater range of luminosities.

For the lowest values of t ($\leq$11), a larger value of $\Delta m_{\,t}(B)$ corresponds to decreasing luminosity (although a degree of degeneracy is still present). The two-part piecewise model (whose tracks can be seen plotted, crossing over in the transitional region) resolves the degeneracy seen in the $\Delta m_{\,15}(B)$ panel. The two distinct tracks, anchored by the calibrator SNe, are continuous, with the flow sample scattering naturally around them.

Intermediate values of t (i.e. $t = 13$ or 15) show a larger value of $\Delta m_{\,t}(B)$ correlating with decreasing luminosity until the knee is met. At this point, the fast decliners show no clear trend, instead displaying a degeneracy wherein differences of $\Delta m_{\,t}(B)$ show no discernable indication of luminosity. At its most extreme, there is over a 2.5 mag difference between points of equal $\Delta m_{\,15}(B)$.

With $t = 20$, the largest value tested in this letter, slow decliners show the same pattern as always (increasing $\Delta m_{\,t}(B)$ correlates with decreasing magnitude). Fast decliners, on the other hand, show the inverse; an increase in $\Delta m_{\,t}(B)$ shows an increase in luminosity. Comparing to $\Delta m_{\,15}(B)$, the break shown by fast decliners in the $t = 20$ plot is far more accentuated. Nevertheless, this extended time-scale does offer a distinct advantage for the normal and slow-declining populations: Their decline-rates become distributed over a significantly wider range of values. This flattens the slope of the relation, meaning that small measurement uncertainties in the decline-rate (e.g. ~ 0.05 mag) have a minimal impact on the derived absolute magnitude.

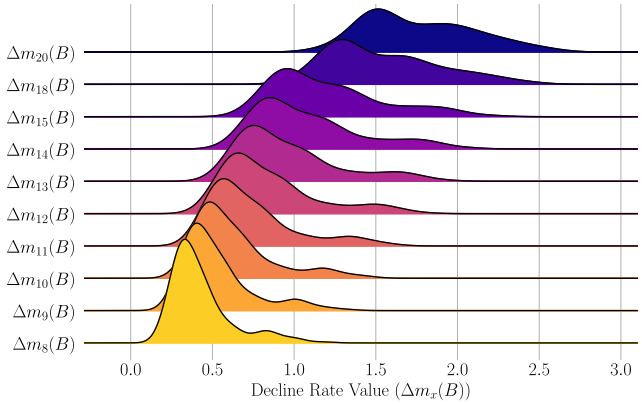


Figure 3. Ridgeline plot showing the distributions of $\Delta m_t(B)$ decline-rates.

We also tested whether these relations hold in the g band, given its similarity in wavelength to the B band and the fact that modern surveys often prefer its use. Results are shown in the bottom panels of Fig. 2. The correlations that are obtained are consistent with their B-band counterparts; the fastest-declining SNe remain degenerate compared to the rest of the data for $t = 15$. $\Delta m_{\,10}(g)$ does present a steeper relation for fast-decliners than $\Delta m_{\,10}(B)$, but despite that a severe degeneracy is still mitigated. Note also that the transitional fast-decliners seamlessly joining the slow-declining track in the g band.

Studying the $\Delta m_{\,t}(B)$ distribution as a whole, Fig. 3 shows a ridgeline plot that demonstrates how the frequency of B band decline-rates changes as the time-scale is altered. For the shortest time-scales, it can be seen that there is one dominant population with a slight knee populated by the fastest-decliners. As the time-scale increases, the dominant population starts to spread over a larger range of values, and the knee becomes more accented, with the fastest-declining SNe separating themselves even further from the larger population. At a time-scale of around 11 d the spread in the dominant population evolves into signs of a second bump, potentially a bimodality in $\Delta m_{\,15}(B)$, as seen in C. Ashall et al. (2016). However, given that the data used here are not a complete, volume-limited sample, such a conclusion is weak. The bump becomes more defined with time until the distribution starts to appear more like three similar, albeit slightly different populations. The dominant population (consisting of the slow-declining extreme and normal Ia's) and the extended knee, corresponding to the fast-decliners, remain clearly defined, while an additional population sitting between the others also becomes more defined.

The SNe populating this region are comprised of faster declining normal SNe Ia, and their behaviour on this plot is fascinating when comparing to their positions on LWR plots for instance (Fig. 2). Where those plots suggest that SNe Ia are separated into groups of 91bg-like and non-91bg-like, the distribution of SNe at the largest time-scales on this plot ($t = 20$ in particular) is in opposition to this conclusion. Instead there appears to be an almost

Downloaded from academic.oup.com/mnras/article/552/4/stag1907/8876083 by Sarah Dakin user on 05 November 2026

continuous distribution where the fastest and slowest-decliners are blended into one another by the fast declining normal Ia's populating the aforementioned bump. One could either look at this as evidence of a continuous class of SN, or instead see it as an example of SNe Ia discontinuity where two (or possibly three) populations are being treated as one.

Though $\Delta m_{\ t}(B)$ for the full range of t is shown in this letter, isolating the most successful decline-rate allows for a more focused comparison against the already established $\Delta m_{\ 15}(B)$. $\Delta m_{\ t}(B)$ where $t \leq 11$ are the clear candidates, resulting from the absence of a defined break section in these plots in Fig. 2 compared to larger values of t.

Another, highly relevant factor concerns the practicality of the approach; simply put, it is easier to get SN data over shorter lengths of time. Compared with $\Delta m_{\ 15}(B)$, for instance, less time coverage is required to compute a $\Delta m_{\ 10}(B)$ value. This means there is less of an opportunity for observing conditions to change which may impact measurements. It also allows for the possibility that previous SNe which lacked sufficient data for $\Delta m_{\ 15}(B)$ can be retrospectively studied should they meet the threshold of $\Delta m_{\ 10}(B)$. While selecting a value of t lower than 10 would even further reduce required data, selecting too short a time range may also lead to unwanted effects. Definition of $t_{X,\max}$ is crucial for ensuring an accurate measurement of light curve decline, and smaller values of t would amplify these potential errors as a lesser value of t is comparatively more difficult to interpolate. The error in defining $t_{X,\max}$ will be constant, irrespective of the choice of t, hence the respective errors increasing.

5 DISCUSSION

Focusing on the chosen value of $t = 10$, a direct comparison of the $\Delta m_{15}(B)$ and $\Delta m_{10}(B)$ LWR plots (Fig. 2) demonstrates the clear advantage of the shorter time-scale. It is worth reiterating the stark difference in fast-decliner behaviour between the two metrics: where the $\Delta m_{15}(B)$ relation exhibits a degenerate vertical break, $\Delta m_{10}(B)$ remains continuous and tracks the full luminosity range. While a transition 'knot' is present, marking the shift to a steeper slope for fast decliners, the severe degeneracy demonstrated with $\Delta m_{15}(B)$ is resolved. Consequently, $\Delta m_{10}(B)$ acts as a superior tool for investigating transitional and fast-declining SNe at the faint end of the luminosity distribution.

This advantage is made clear by plotting the two decline-rates directly against one another (Fig. 4). For normal SNe Ia ($\Delta m_{15}(B) < 1.6$ mag), there is a tight linear correlation between $\Delta m_{10}(B)$ and $\Delta m_{15}(B)$, confirming that these parameters can be safely converted into one another for slow and normal decliners. These conversions are defined as follows:

$$\Delta m_{10}(B) = 0.602 \cdot \Delta m_{15}(B) - 0.113, \quad (1)$$
$$\Delta m_{10}(g) = 0.574 \cdot \Delta m_{15}(g) - 0.065. \quad (2)$$

However, as SNe cross the empirical fast-declining threshold, they deviate from this linearity. Because $\Delta m_{10}(B)$ maintains a continuous correlation with absolute magnitude, the clear break in linearity, seen in Fig. 4, confirms that $\Delta m_{15}(B)$ loses discerning power for fast-declining events. As shown in the bottom panels of Fig. 4, these exact trends are identically mirrored in the g band.

To standardise SN Ia luminosities using $\Delta m_{10}(X)$, we fit the LWR using continuous piecewise linear models (plotted in Fig. 5). The transition knots where the normal track meets the fast-declining track were empirically determined by our calibrator sample to be $\Delta m_{10}(B) = 0.89$ mag and $\Delta m_{10}(g) = 1.10$ mag.

For the B band, the absolute magnitude is given by

$$M_B = \begin{cases} -19.322 + 0.617\,(\Delta m_{10}(B) - 0.60), & \text{if } \Delta m_{10}(B) < 0.89, \\ -19.143 + 4.208\,(\Delta m_{10}(B) - 0.89), & \text{if } \Delta m_{10}(B) \geq 0.89. \end{cases} \quad (3)$$

For the g band, the absolute magnitude is given by

$$M_g = \begin{cases} -19.101 + 1.585\,(\Delta m_{10}(g) - 0.60), & \text{if } \Delta m_{10}(g) < 1.10, \\ -18.309 + 7.649\,(\Delta m_{10}(g) - 1.10), & \text{if } \Delta m_{10}(g) \geq 1.10. \end{cases} \quad (4)$$

The intrinsic root-mean-square (RMS) scatter around the normal, slow-declining track of our piecewise model is remarkably low: 0.08 mag in the B band and 0.12 mag in the g band. This confirms that $\Delta m_{10}(X)$ is a highly precise proxy for standardising normal SNe Ia. For comparison, fitting this exact same calibrator sample using the traditional $\Delta m_{15}(X)$ parameter yields a larger normal-regime scatter of 0.19 mag in the B band and 0.30 mag in the g band.

For the fast-declining tail ($\Delta m_{15}(B) \geq 1.6$ mag), the intrinsic dispersion naturally increases, rising to 0.34 mag in the B band and 0.40 mag in the g band. However, this is a vast improvement over $\Delta m_{15}(X)$, which completely degenerates in this regime, yielding a RMS scatter of 0.94 and 0.75 mag in the B and g bands, respectively. While the piecewise model prevents these faint objects from breaking the overall calibration, this scatter is noticeably larger than the 0.19 mag RMS error achieved by M. M. Phillips et al. (2026) when s_{BV} is used as the light curve width indicator for fast decliners. This indicates that while Δm_{10} is an excellent, short-baseline standardisation tool for normal SNe Ia, multiband colour-stretch parameters like s_{BV} remain superior for precisely resolving the luminosities of the fastest-declining events.

It is interesting to compare $\Delta m_{10}(X)$ and the colour-stretch parameters, s_{BV} and s_{gr} (C. R. Burns et al. 2014; C. Ashall et al. 2020). Colour-stretch parameters are highly capable of tracking SN Ia brightness across the full magnitude range by utilising multiband colour evolution. Shown in Fig. 5 is a comparison of $\Delta m_{10}(B)$ and s_{BV} when plotted against M_B. While the correlations displayed are not identical, $\Delta m_{10}(B)$ offers a close approximation to the results of s_{BV}, despite its minimal data requirements. Fig. 4 shows that $\Delta m_{\ 10}(B)$ smoothens the delineation caused by $\Delta m_{\ 15}(B)$ with s_{BV} (Velasco et al., in preparation). Furthermore, the relationship between $\Delta m_{10}(g)$ and s_{gr} (Fig. 4) appears even tighter than its B-band counterpart across the entire luminosity range, suggesting that for slow declining SNe $\Delta m_{10}(B)$ may be advantageous when compared to s_{BV}.

This comparative behaviour extends to the g band. As shown in Fig. 5, $\Delta m_{10}(g)$ also provides a strong approximation of its corresponding colour-stretch parameter, s_{gr}. While colour-stretch parameters definitively perform better when tracking the luminosities of the fastest-declining SNe Ia at the faint end of the distribution, $\Delta m_{10}(X)$ provides a complementary alternative for the slow-decliners. When employed as a fast, low-effort tool, $\Delta m_{10}(X)$ has the capacity to replicate the standardisation power of a much more complex parameter.

As a final caveat, it should be noted that while our piecewise model successfully maps normal and fast-declining SNe, the peculiar SNe Ia-03fg are known outliers to many standardisation techniques (D. A. Howell et al. 2006; C. Ashall et al. 2021). For instance, while their slow decline-rates result in high predicted luminosities under our Δm_{10} framework, objects such as ASASSN-

Downloaded from academic.oup.com/mnras/article/552/4/stag1907/8876083 by Sarah Dakin user on 05 November 2026

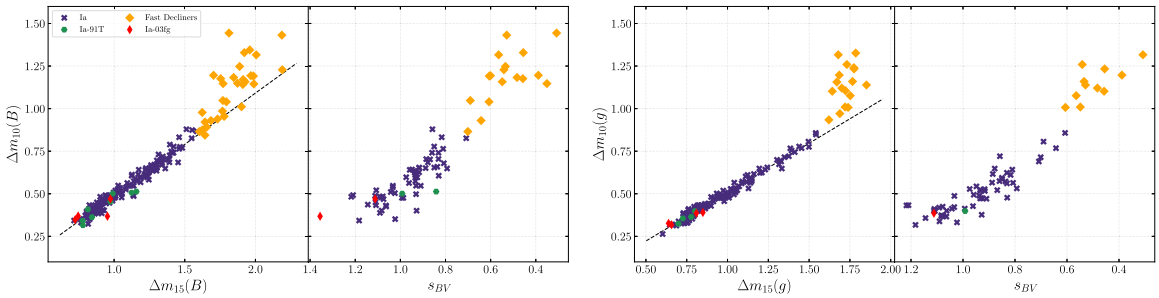


Figure 4. Direct comparisons of decline-rate and colour-stretch parameters. The panels are arranged horizontally, with the left two panels displaying B-band comparisons and the right two displaying g-band comparisons. From left to right, the panels show: $\Delta m_{10}(B)$ versus $\Delta m_{15}(B)$, $\Delta m_{10}(B)$ versus s_{BV}, $\Delta m_{10}(g)$ versus $\Delta m_{15}(g)$, and $\Delta m_{10}(g)$ versus s_{BV}. A linear relation (dashed line) is fitted to the normal SNe Ia ($\Delta m_{15}(B) < 1.6$ mag) in the $\Delta m_{15}(X)$ panels to highlight the tight correlation for normal decliners, which breaks down for the fast-declining tail (orange diamonds). A legend detailing the subclass markers is provided in the far-left panel.

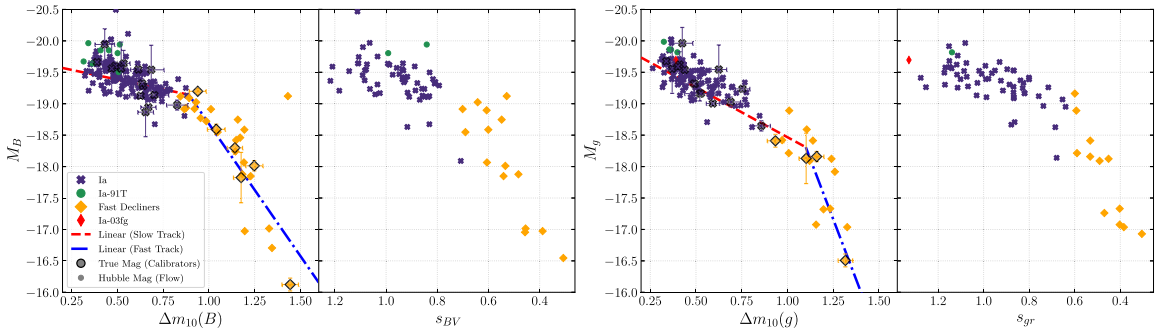


Figure 5. Calibrated absolute magnitudes plotted against Δm_{10} and colour-stretch parameters. The left two panels display M_B versus $\Delta m_{10}(B)$ and s_{BV}, respectively. The right two panels display M_g versus $\Delta m_{10}(g)$ and s_{gr}, respectively. True empirical calibrator SNe are plotted with bold black marker outlines and error bars. As in Fig. 2, the broader 'flow' sample is plotted as a faded background distribution utilising independent Hubble distances, with their error bars omitted for clarity. The derived continuous piecewise linear models (red for the normal track, blue for the fast track) are shown on the Δm_{10} panels.

15hy are physically underluminous (J. Lu et al. 2021). As such they remain highlighted as a distinct subclass in our analysis.

6 CONCLUSIONS

We presented an explorative study of SNe Ia decline-rates utilising the $\Delta m_t(X)$ metric to evaluate alternative parameterisations of light curve diversity and the LWR. The primary advantage of $\Delta m_{10}(X)$ is not computational speed, but rather that it provides a robust, empirical indicator of light-curve width across the full range of decline-rates without resorting to template fitting. By requiring only 10 d of post-maximum photometric coverage, $\Delta m_{10}(X)$ can be a highly practical tool for large-scale photometric surveys. It allows for rapid characterisation and absolute magnitude estimation with minimal data, making it a practical complement to more data-intensive metrics.

Our analysis confirms that while the traditional $\Delta m_{15}(B)$ parameter suffers from a degeneracy at the faint end of the luminosity distribution, $\Delta m_{10}(X)$ successfully mitigates this break, maintaining a continuous correlation with luminosity for both the B and g bands.

However, we find that the intrinsic dispersion of the LWR is still dominated by the fast-declining tail ($\Delta m_{15}(B) \geq 1.6$ mag). Because these rapidly evolving events (a regime encompassing both 1986G-like and 1991bg-like SNe) synthesise less ^{56}Ni and exhibit fundamentally cooler, distinct photometric evolution (P. A. Mazzali et al. 1997), they cannot simply be modelled as a linear extension of normal SNe Ia. Instead, they must be treated with a distinct calibration track. The chosen piecewise model successfully handles this transition without breaking the calibration, aligning with recent literature that also separately treats fast-decliners (O. Graur 2024; M. M. Phillips et al. 2026).

Although $\Delta m_{10}(B)$ and s_{BV} exhibit a tight relationship (Velasco et al., in preparation), they possess distinct observational strengths. While multiband colour-stretch parameters like s_{BV} remain optimal for luminosity estimates of the faintest, fastest-declining SNe, $\Delta m_{10}(X)$ performs just as well, if not better, for the slow-declining extreme. With intrinsic dispersions of just $\sigma = 0.08$ mag (B band) and 0.12 mag (g band) for normal SNe Ia, $\Delta m_{10}(X)$ provides a highly precise, short-baseline alternative for standardising the vast majority of the SN Ia population.

ACKNOWLEDGEMENTS

The work of the CSP-II has been generously supported by the National Science Foundation under grants no. AST-1008343, AST-1613426, AST-1613455, and AST-1613472. The CSP-II was also supported in part by the Danish Agency for Science and Technology and Innovation through a Sapere Aude Level 2 grant. LG acknowledges financial support from CSIC, MCIN,and AEI 10.13039/501100011033 under projects PID2023-151307NB-I00, PIE 20215AT016, CEX2020-001058-M, and by the MaX-CSIC Ex-

Downloaded from academic.oup.com/mnras/article/552/4/stag1907/8876083 by Sarah Dakin user on 05 November 2026

cellence Award MaX4-SOMMA-ICE. MDS acknowledges support from the Independent Research Fund Denmark (IRFD; grant no. 10.46540/2032-00022B). This research was supported by the Science and Technology Facilities Council (STFC) grants, whom JMV would like to thank.

Facilities: *Magellan*:Baade (IMACS imaging spectrograph, FourStar wide-field near-infrared camera, FIRE near-infrared echellette), *Magellan*:Clay (LDSS3 imaging spectrograph), Swope (SITe3 CCD imager, e2v 4 K × 4 K CCD imager), du Pont (Tek5 CCD imager, WFCCD imaging spectrograph, RetroCam near-infrared imager), Gemini:North (GNIRS near- infrared spectrograph), Gemini:South (FLAMINGOS2), VLT (ISAAC, MUSE), IRTF (SpeX near-infrared spectrograph), NOT (ALFOSC), Calar Alto 3.5 m (PMAS/PPak), La Silla-QUEST (CRTS, PTF, iPTF, OGLE, ASAS-SN, PS1, KISS, ISSP, MASTER, SMT).

Software: SNID (S. Blondin & J. L. Tonry 2007), SUPERFIT (D. A. Howell et al. 2005), GELATO (A. H. Harutyunyan et al. 2008), and SNOOPY (C. R. Burns et al. 2011, 2014).

DATA AVAILABILITY

The CSP-I DR3 data used for this work are available at the Carnegie Supernova Project's respective website. CSP-II data are being released alongside relevant papers, though the whole survey in totality is still private. The data sets specifically curated for the analysis section, can be shared on reasonable request to the corresponding author.

REFERENCES

Alburai A. et al., 2026, A&A, 707, A91
Ashall C., Mazzali P., Sasdelli M., Prentice S. J., 2016, MNRAS, 460, 3529
Ashall C. et al., 2020, ApJ, 895, L3
Ashall C. et al., 2021, ApJ, 922, 205
Blakeslee J. P., Jensen J. B., Ma C.-P., Milne P. A., Greene J. E., 2021, ApJ, 911, 65
Blondin S., Tonry J. L., 2007, ApJ, 666, 1024
Burns C. R. et al., 2011, AJ, 141, 19
Burns C. R. et al., 2014, ApJ, 789, 32
Burns C. R. et al., 2018, ApJ, 869, 56
Fitzpatrick E. L., 1999, PASP, 111, 63
Folatelli G. et al., 2010, AJ, 139, 120
Graur O., 2024, MNRAS, 530, 4950
Hamuy M., Phillips M. M., Suntzeff N. B., Schommer R. A., Maza J., Aviles R., 1996, AJ, 112, 2391
Harutyunyan A. H. et al., 2008, A&A, 488, 383
Hoeflich P. et al., 2017, ApJ, 846, 58
Howell D. A. et al., 2005, ApJ, 634, 1190
Howell D. A. et al., 2006, Nature, 443, 308
Hoyle F., Fowler W. A., 1960, ApJ, 132, 565
Jensen J. B. et al., 2021, ApJS, 255, 21
Jha S., Riess A. G., Kirshner R. P., 2007, ApJ, 659, 122
Krisciunas K. et al., 2017, AJ, 154, 211
Livio M., Mazzali P., 2018, Phys. Rep., 736, 1
Lu J. et al., 2021, ApJ, 920, 107
Mazzali P. A., Chugai N., Turatto M., Lucy L. B., Danziger I. J., Cappellaro E., Delia Valle M., Benetti S., 1997, MNRAS, 284, 151
Mazzali P. A., Röpke F. K., Benetti S., Hillebrandt W., 2007, Science, 315, 825
Perlmutter S. et al., 1998, Nature, 391, 51
Perlmutter S. et al., 1999, ApJ, 517, 565
Phillips M. M., 1993, ApJ, 413, L105
Phillips M. M., Burns C. R., 2017, The Peak Luminosity–Decline Rate Relationship for Type Ia Supernovae, Springer International Publishing, Cham, p. 2543
Phillips M. M., Lira P., Suntzeff N. B., Schommer R. A., Hamuy M., Maza J., 1999, AJ, 118, 1766
Phillips M. M. et al., 2018, PASP, 131, 014001
Phillips M. M. et al., 2022, ApJ, 938, 47
Phillips M. M. et al., 2026, ApJ, 998, 101
Pskovskii I. P., 1977, Sov. Astron., 21, 675
Riess A. G. et al., 1998, AJ, 116, 1009
Riess A. G. et al., 1999, AJ, 117, 707
Riess A. G. et al., 2022, ApJ, 934, L7
Schlafly E. F., Finkbeiner D. P., 2011, ApJ, 737, 103
Taubenberger S. et al., 2008, MNRAS, 385, 75
Tripp R., 1998, A&A, 331, 815
Tully R. B., Rizzi L., Shaya E. J., Courtois H. M., Makarov D. I., Jacobs B. A., 2009, AJ, 138, 323
Tully R. B. et al., 2023, ApJ, 944, 94
Uddin S. A. et al., 2024, ApJ, 970, 72
Wang B., Han Z., 2012, New Astron. Rev., 56, 122

This paper has been typeset from a TEX/LATEX file prepared by the author.

Downloaded from academic.oup.com/mnras/article/552/4/stag1907/8876083 by Sarah Dakin user on 05 November 2026

© The Author(s) 2026.
Published by Oxford University Press on behalf of Royal Astronomical Society. This is an Open Access article distributed under the terms of the Creative Commons Attribution License (https://creativecommons.org/licenses/by/4.0/), which permits unrestricted reuse, distribution, and reproduction in any medium, provided the original work is properly cited.